A versatile instrument with an optical parametric oscillator transmitter tunable from 1.5 to 3.1 m for aerosol lidar and DIAL

A versatile instrument with an optical parametric oscillator transmitter tunable from 1.5 to 3.1 μm for aerosol lidar and DIAL

Iain Robinson[a], Jim W. Jack[a], Cameron F. Rae[b] and John Moncrieff*[a]

[a]School of Geosciences, University of Edinburgh, The King's Buildings, West Mains Road, Edinburgh, Scotland, UK, EH9 3JN; [b]Photonics Innovation Centre, School of Physics and Astronomy, University of St Andrews, North Haugh, St Andrews, Fife, Scotland, UK, KY16 9SS

ABSTRACT

Lidar is a valuable tool for atmospheric monitoring, allowing range-resolved profile measurements of a variety of quantities including aerosols, wind, pollutants and greenhouse gases. We report here the development of a versatile field-deployable instrument for monitoring the lower troposphere. This region includes the effects of surface–atmosphere interactions and is an area where the resolution of satellite data is generally poor.

Our instrument has been designed with the goal of making range-resolved measurements of greenhouse gases such as carbon dioxide, as well as probing the structure of the boundary layer. The key component is a tunable laser source based on an optical parametric oscillator covering the wavelength range 1.5–3.1 μm. This relatively eye-safe spectral region includes absorption lines of carbon dioxide and other greenhouse gases enabling the application of the differential absorption lidar (DIAL) technique, whilst also being suitable for aerosol lidar. We also report the use of an avalanche photodiode detector with high sensitivity and low noise.

Field tests of the instrument were performed, recording continuous lidar signals over extended periods. The data were digitized at up to 8 signals per second. Scattering from aerosols and molecules was detected to a maximum range of 2 km, whilst scattering from cloud was recorded at up to 6 km. The data are plotted as time-versus-range images to show the dynamic state of the atmosphere evolving over time.

These results demonstrate that the lidar achieves key requirements for both aerosol scatter and DIAL: tunability of the transmitter wavelength, sensitivity to molecular and aerosol scattering and robustness for field use.

Keywords: lidar, DIAL, differential absorption, laser, OPO, avalanche photodiode, APD, HITRAN

1. INTRODUCTION

Climate change and air pollution are driving demand for improved atmospheric data to aid the scientific understanding of these problems and assess the effectiveness of mitigation strategies. New instruments are needed to meet this demand for high-quality data whilst being both robust and inexpensive. Static sensors are capable of high precision in situ environmental monitoring however cost considerations mean that measurement networks are inevitably sparse[1]. Quantitative results derived from models based on spatially sparse data are inherently limited in accuracy. Data sampled by aircraft cover a wider area, but are too costly to deploy routinely. Satellites give global coverage but have poor accuracy in the boundary layer.

Lidar is a powerful technique that can bridge the gap by providing measurements with spatial resolution. In lidar a pulse of laser light is fired through the atmosphere and the signal returning back to the instrument is recorded over time. The temporal profile of this back-scattered signal gives the range (distance) at which the light is scattered by molecules or particles in the air. It is this feature which gives lidar its spatial resolution. The definitive reference on lidar is Measures' 1984 textbook[2], and a comprehensive overview of modern applications is given by Weitkamp[3]. A variety of techniques have been developed to enable lidar to make quantitative measurements of atmospheric constituents. Aerosol lidar is used to monitor particles such as smoke from forest fires[4] or air pollution[5]. Differential absorption lidar[6] (DIAL) enables measurement of water vapour[7], pollutants[8] and trace gases[9].

Recent progress in these techniques is leading to further new applications for lidar. At the same time, developments in laser science and telecommunications are improving the versatility and robustness of lasers, whilst also reducing their

*J.Moncrieff@ed.ac.uk; phone +44 131 650 5402

Lidar Technologies, Techniques, and Measurements for Atmospheric Remote Sensing IX, edited by Upendra N. Singh, Gelsomina Pappalardo, Proc. of SPIE Vol. 8894, 88940L
 · doi: 10.1117/12.2029164

cost. This robustness is crucial both for field use of portable instruments and in long-term monitoring set-ups. Developments in laser diodes, diode-pumped solid state systems and fibre lasers are particularly significant.

We describe here a lidar we have developed using a solid-state laser source based on an optical parametric oscillator (OPO). An OPO uses non-linear effects in a crystal to convert light at one wavelength to another. The output wavelength is pulsed and tunable (often by rotating the crystal) and therefore provides opportunities for a range of lidar applications.

The need for improved measurements of greenhouse gases motivated our development of this instrument. This could aid understanding of the global carbon cycle and improve the accuracy of emissions inventories, but also has potential in applications for monitoring specific sources such as landfill[10], carbon capture and storage[11] and leaks from industrial sites[12].

DIAL is the lidar technique best-suited to making greenhouse gas measurements. Our goal is to use DIAL to make measurements of carbon dioxide (CO_2) concentration and this will be the focus of this paper. Section 2 provides an outline of the DIAL technique, and discusses the choice of laser wavelength for CO_2. Section 3 describes the the development of the instrument and Section 4 presents the results of its first field tests.

2. DIFFERENTIAL ABSORPTION LIDAR (DIAL)

In a DIAL measurement, pulses at two carefully-selected wavelengths are fired into the atmosphere sequentially. The first at the off-line wavelength, λ_{off}, is scattered in the atmosphere, the second at the on-line wavelength, λ_{on}, is absorbed as well as scattered. If the differential absorption cross section, $\sigma(\lambda_{on})-\sigma(\lambda_{off})$, is known, the concentration of the absorbing gas as a function of range may be calculated[6]. The process of using two wavelengths removes dependencies on instrumental parameters and the atmospheric backscatter coefficient, provided that these values remain unchanged whilst switching the laser output between the on-line and off-line wavelengths.

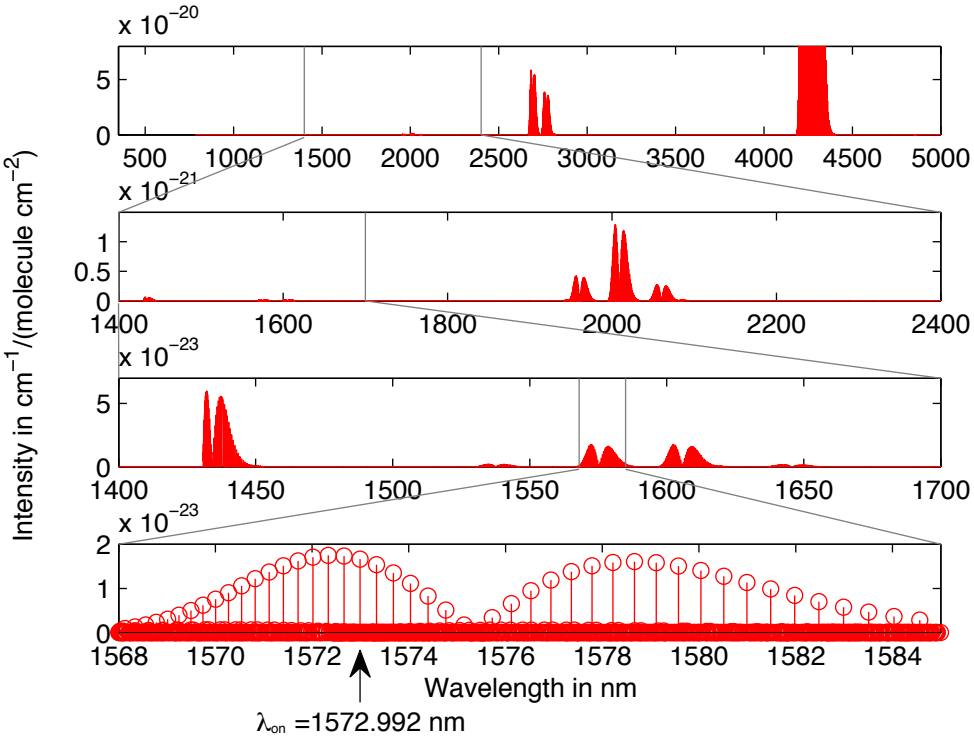

Figure 1. An overview of the positions and intensities of lines in the absorption spectrum of the $^{16}O^{12}C^{16}O$ isotopologue of carbon dioxide. The data are from the HITRAN 2008 database[13]. The selected on-line wavelength (λ_{on}) for DIAL is also shown.

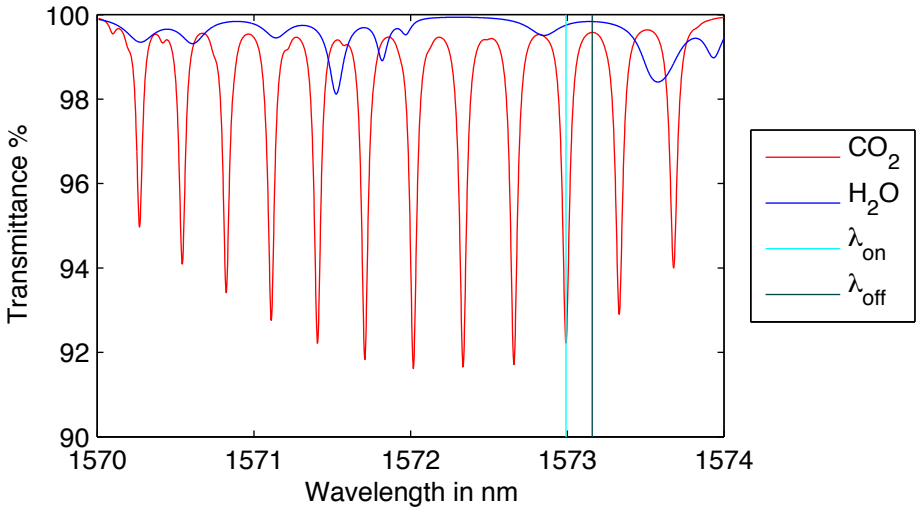

Figure 2. Simulation of the spectral transmittance of the atmosphere over a path length of 2 km for a pressure of 1 atm with a carbon dioxide (CO_2) concentration of 314 µmol/mol. The transmittance of water (H_2O) at 4 % abundance is also shown.

To measure CO_2 the on-line wavelength must be precisely tuned to match a line in its absorption spectrum. At the same time the off-line wavelength must suffer minimal absorption, both by CO_2 and by other interfering gases such as water vapour. The High-resolution Transmission database (HITRAN) provides spectroscopic parameters that can be used to identify absorption lines, and calculate or simulate an absorption spectrum. Figure 1 shows an overview of CO_2 absorption lines from the 2008 edition[13] of the database. Only the most abundant isotopologue is shown, $^{16}O^{12}C^{16}O$, which has a natural abundance of 98.4 %.

The choice of wavelength is motivated by several factors. For eye safety, infrared wavelengths above 1.4 µm are preferred as the maximum permissible exposure is relatively high in this spectral region[14]. Gibert[15] and Refaat[16] have built DIAL instruments using CO_2 absorption lines near 2 µm. Due to limited options for detectors in this wavelength region heterodyne detection is generally required. Sakaizawa[17] has demonstrated CO_2 DIAL using an absorption line near 1570 nm and Amediek[18] and Abshire[19] have made integrated path measurements in this spectral region. Although these absorption lines are substantially weaker than the lines near 2 µm (see Figure 1) this wavelength has the advantage that high-sensitivity direct detection sensors are available. The use of this spectral region for telecommunications means that devices such as detectors, coated optics and other components are relatively inexpensive and generally available off-the-shelf.

The on-line wavelength used by Amediek[18], 1572.993 nm, is labelled in Figure 1. The HITRAN database gives the (half) width of this line (at a pressure of 1 atm) as 2.34 GHz (19.3 pm). To relate the HITRAN parameters to the spectral transmittance of the atmosphere the absorption spectrum must be simulated. The tool *HITRAN on the Web*[20] simulates the transmittance of the atmosphere using HITRAN parameters and atmospheric variables. The results of a simulation are shown in Figure 2 for a 2 km path through an atmosphere (1 atm) with 314 µmol/mol (parts per million) CO_2 concentration. The transmittance at the on-line wavelength is 92.2 %. At the off-line wavelength shown, 1573.16 nm, the transmittance is 99.6 %. The spectrum of water at 4 % abundance is also shown as it is a potential interfering species.

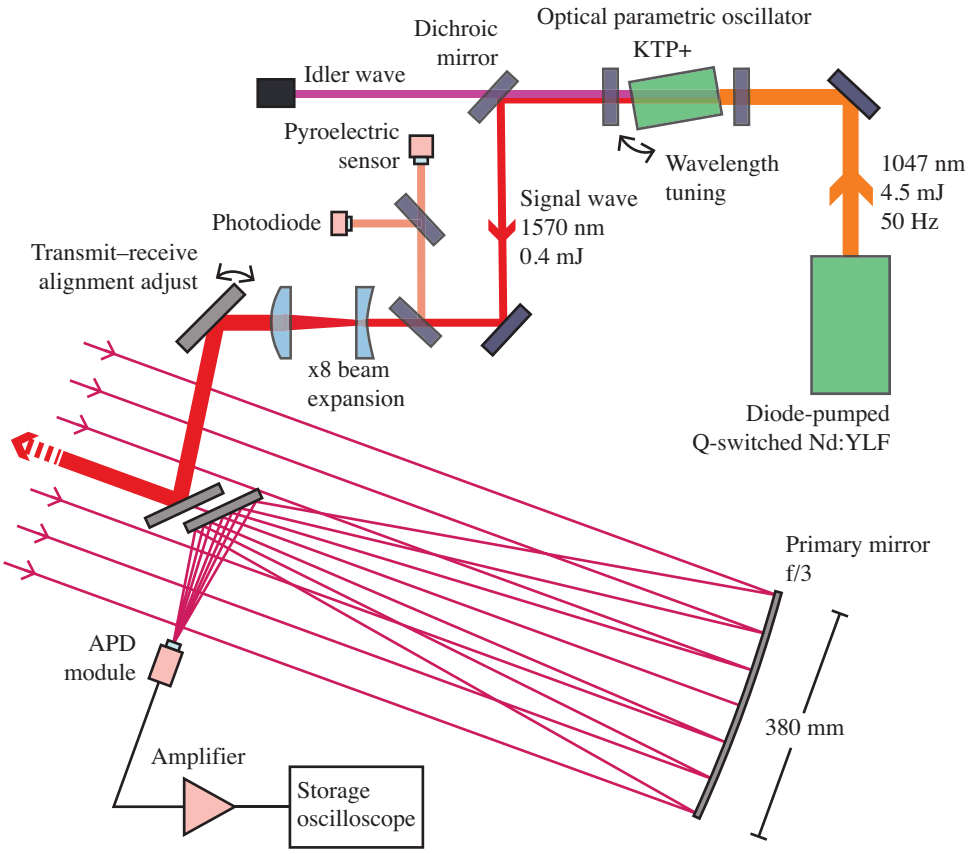

Figure 3. Diagram of the lidar instrument. The optical parametric oscillator, with a potassium titanyl phosphate (KTP+) non-linear crystal, is pumped by a Q-switched neodymium-doped yttrium lithium fluoride (Nd:YLF) laser. The signal wave is separated by a dichroic mirror and expanded before transmission through the atmosphere along the axis of a Newtonian telescope. The received signal is focused into an avalanche photodiode (APD) module.

3. THE LIDAR INSTRUMENT

The instrument consists of a laser transmitter, receiver telescope and detector, shown in Figure 3.

A diode-pumped neodymium-doped yttrium lithium fluoride (Nd:YLF) laser provides a pump wavelength of 1047 nm. The Nd:YLF laser is Q-switched and emits pulses of 4.5 mJ energy at a repetition rate of 50 Hz. The OPO non-linear crystal is potassium titanyl phosphate (KTP+) with type-II non-critical phase matching. The OPO shifts the pump wavelength to signal and idler wavelengths near 1.5 µm and 3.1 µm respectively. These wavelengths are tunable (though not independently) by rotating the crystal. The conversion efficiency from the pump laser to the signal and idler waves was measured as 21 %. The signal wavelength at 1570 nm was separated from the idler by reflection from a dichroic mirror. The pulse duration (full width at half maximum) was measured as 4.6 ns with a fast photodiode and the pulse energy in the signal wave was 0.39 mJ. For the experiments described here the idler wavelength (3 µm) was not used. Part of the signal wave was picked off to monitor the energy of each transmitted pulse with pyroelectric sensor (PY-ITV-SINGLE-TO39(2+1), Pyreos). An indium gallium arsenide (InGaAs) PIN photodiode (G8370-05, Hamamatsu) was used to provide a timing reference signal for triggering the signal acquisition. The divergence of the signal wave was measured as 5.1 mrad. After expanding the beam by a factor of 8, this is reduced to 0.6 mrad.

The beam was transmitted into the atmosphere along the axis of a custom-built Newtonian telescope. The telescope has a 380 mm diameter primary mirror with a 1150 mm focal length (f/3) and a 130 mm diameter planar secondary mirror. The received signal was detected with an avalanche photodiode (APD) module (C30659-1550-R2AHS, Excelitas) consisting of a 200 µm diameter InGaAs APD with an integrated low-noise preamplifier and 50 MHz bandwidth. A bias voltage of 48.4 V was applied to the APD. At this voltage the specified response of the module is 340 mV/µW. The

module is AC coupled, removing any constant background from the signal. The module output was amplified by a two-stage voltage amplifier (AD8066, Analog Devices) with a total gain of 29 and a bandwidth of 24 MHz. The signal was digitized by a storage oscilloscope (WaveSurfer 454, LeCroy) at a sample rate of 2 GS/s. The final bandwidth of the signal is determined by the slowest system, the voltage amplifier (24 MHz). The rise time of this amplifier is 15 ns, giving the instrument a range resolution of 2.2 m.

The small size of the detector restricts the field of view of the telescope to 0.17 mrad. This is less than the beam divergence of 0.6 mrad, resulting in less-than-ideal overlap of the transmit and receive channels. The beam may be expanded further to reduce the divergence to within the telescope field of view. The maximum expansion is limited only by the diameter of the secondary mirror (130 mm) which is 92 mm when projected at 45° along the telescope axis.

4. RESULTS AND DISCUSSION

Field tests of the instrument were undertaken to determine its performance and stability by recording the back-scatter signal over periods of up to half an hour. Figure 4 shows the location of the measurement site as well as the beam direction and elevation (20°). A typical return signal is shown in Figure 5. The measurement was made on a cloudy night. The transmitter pulse energy was 0.39 mJ and the lidar return signal was averaged over 50 pulses, to give one lidar signal per second. The optical power (in nW) was calculated from the specified response of the APD module and the calculated gain the amplifier circuit.

Little signal is detected for the first 200 m. This is largely due to the beam remaining within the shadow of the secondary mirror preventing the telescope from efficiently focusing the return signal within this range. The beam begins to emerge from this shadow around 200 m, and the return signal intensity reaches a maximum around 350 m. Beyond this the signal starts to fall off due to its dependence on the inverse square of the range. The obscuration caused by the secondary mirror is a feature of Newtonian telescopes and due in part to the small size (0.2 mm diameter) of the detector. Using a larger detector, a 1 mm diameter PIN photodiode (G8370-01, Hamamatsu), we observed this peak at 140 m range. However, the optical limitations on the telescope imposed by the small size of APDs are outweighed by the advantage of their higher sensitivity.

The return signal up to 920 m is due to atmospheric scattering by molecules and aerosols[6]. At this infrared wavelength, we expect aerosol scattering to be the dominant contribution. Around 1 km from the instrument (375 m altitude at a 20° slant), a strong return signal from cloud was detected. Immediately after this peak, the signal becomes slightly negative. This is caused by overshoot of the detector and is due to the limited bandwidth (24 MHz) of the detector amplifier and also the fact that the signal is AC coupled. This kind of overshoot and related ringing effects are commonly observed in lidar signals from cloud[21,22]. The maximum range from which cloud scattering could be detected was 5.7 km, indicating that the beam quality is sufficient for longer-range propagation.

The noise level of the detector during field tests was found by measuring the standard deviation of the detector signal before the laser fired, giving a value of 110 pW. With averaging over 50 pulses, the specified detector noise in a 24 MHz bandwidth is expected to be in the range 60 to 113 pW, indicating that the detector achieved its specified noise performance.

To study variation in the atmosphere over time lidar signals were recorded continuously over an interval of 9 min. The signals are shown in Figure 6 as a time-versus-range image with a colour scale giving the optical power of the return signal.

The atmospheric scattering signal can be seen in the image between 200 and 1000 m. There are some significant variations (>10 %) in this this signal over time, particularly at 1.3 and 5.2 min. These fluctuations, which occur on a timescale of several seconds, may be due to turbulence in the surface layer. This turbulence may be more pronounced as the beam path lies directly over a hill (Blackford Hill), passing approximately 250 m above the summit.

Figure 4. The instrument measurement site was at the University of Edinburgh (55° 55' 22" N, 3° 10' 42" W) and the laser was directed westwards (273°) with an elevation angle of 20° to the horizontal.

There are a number of features visible in the region between 600 and 550 m which may be due to aerosol plumes passing through the beam or rain descending from the cloud layer. Their slanted appearance suggests that material is moving away from the instrument over time. This is consistent with a measurement of wind direction made at the time by a weather station (280 m from the instrument and 20 m higher) which reported an easterly wind (78°) at 2.4 m/s. The features appear to be wider at greater height. The mean wind velocity is expected to increase logarithmically with height[23], so this could be causing material to disperse quicker at higher altitudes.

It was found that the transmit–receive channel alignment was susceptible to drift. On some days this occurred over a timescale of minutes, whilst on others it was stable for over half an hour. The drift is likely caused by the inevitable temperature fluctuations in an outdoor environment. This issue may be remedied by improving the instrument's mechanical stability and temperature control. Use of fibre delivery where possible may isolate the instrument from misalignments in individual systems.

These measurements demonstrate the feasibility of using the instrument to examine the structure and evolution of the boundary layer, as well as for cloud and aerosol detection. The temporal resolution (1 s) and spatial resolution (2.2 m) of the instrument make it applicable to the study of micrometeorological phenomena.

For DIAL measurements it is imperative that the return signal is constant whilst switching between the on-line and off-line wavelengths. These results therefore illustrate the importance of a fast (sub-second) switching speed. Further work is now underway to narrow the spectral width of the laser output to be able to target a specific CO_2 absorption line by injection seeding the OPO with a frequency-stabilized diode laser locked to the online wavelength[17,18,24].

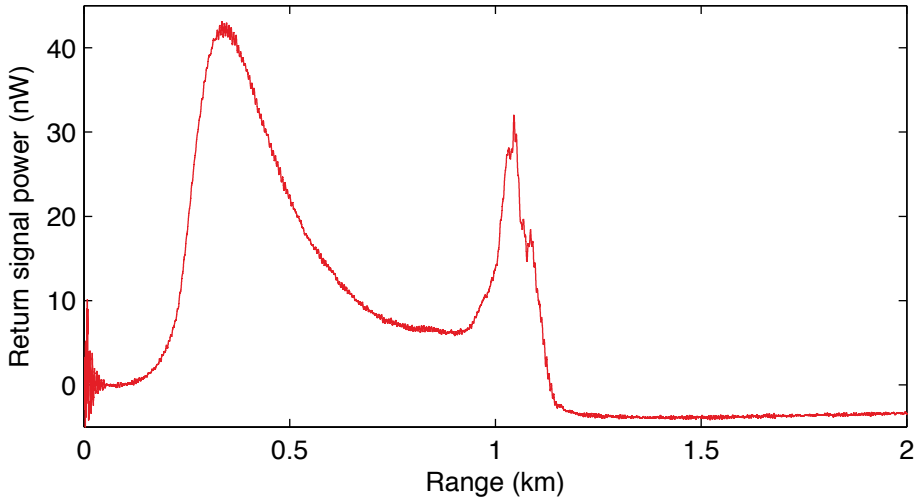

Figure 5. Return signal measured during lidar field test. The instrument was directed at an elevation of 20° to the horizontal. The signal around 1 km is due to cloud. The transmit pulse energy was 0.39 mJ.

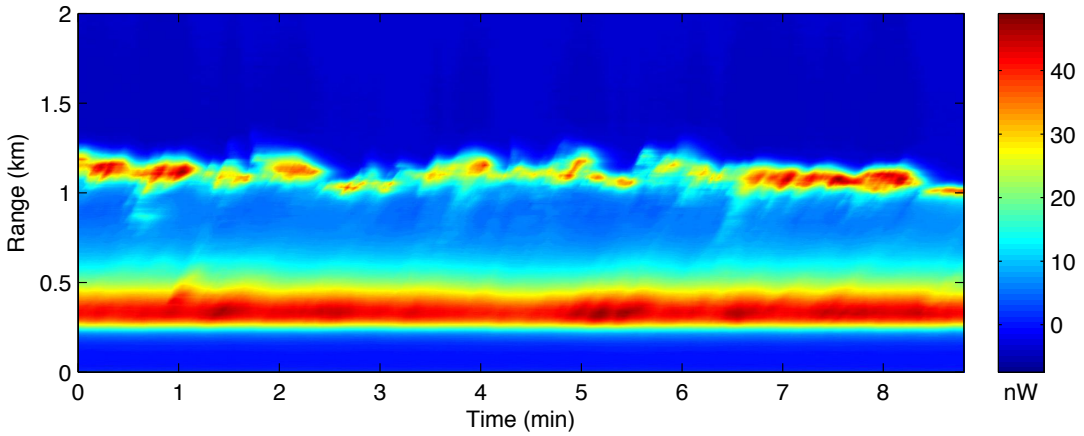

Figure 6. A time-versus-range image showing variation in the return signal optical power (colour scale) over an interval of 9 min. The signals were recorded at night (starting at 22:48 UTC) on 7th March 2013. The location and direction of the beam are indicated in Figure 4.

5. CONCLUSIONS

A versatile field-deployable lidar instrument based on an optical parametric oscillator laser source and avalanche photodiode detector has been developed. Field tests of the instrument were conducted recording the lidar signal over a 9 min interval. Atmospheric scattering was detected from ranges up to 2 km, and cloud scattering from up to 6 km. The results demonstrate the utility of the instrument for studying dynamic structures in the boundary layer as well as the versatility of using a tunable laser source in the eye-safe region. The laser source also covers the spectral range of absorption lines of carbon dioxide and will be adapted to meet the demands of differential absorption lidar.

ACKNOWLEDGEMENTS

This work was partly funded by The University of Edinburgh under a Development Grant with support from an EU FP7 programme "InGOS - Non CO_2 GHG Balance of Europe (INFRA-2011-1.1.11)". We are grateful to Martin Reekie for assistance with the design of the detector amplifier.

REFERENCES

[1] Marquis, M. and Tans, P., "Carbon Crucible," Science 320(5875), 460–461 (2008). doi:10.1126/science.1156451

[2] Measures, R. M., [Laser Remote Sensing: Fundamentals and Applications], Krieger Publishing Company, Malabar (1992).

[3] Weitkamp, C. (ed.), [Lidar: Range-Resolved Optical Remote Sensing of the Atmosphere], Springer, New York (2005). doi:10.1007/b106786

[4] Gaudio, P., Gelfusa, M., Lupelli, I., Malizia, A., Moretti, A., Richetta, M., Serafini, C. and Bellecci, C. "First open field measurements with a portable CO_2 lidar/ dial system for early forest fires detection," Proceedings of SPIE 8182, 818213–1–7 (2011). doi:10.1117/12.898082

[5] Mayor, S., and Spuler, S. M., "Raman-shifted eye-safe aerosol lidar," Applied Optics 43(19), 3915–3924 (2004). doi:10.1364/AO.43.003915

[6] Collis, R. T. H. and Russell, P. B., "Lidar Measurement of Particles and Gases by Elastic Backscattering and Differential Absorption," in Hinkley, E. D. (ed.), [Laser Monitoring of the Atmosphere], Springer-Verlag, Berlin (1976). doi:10.1007/3-540-07743-X

[7] Bösenberg, J., "Differential-absorption lidar for water vapor and temperature profiling," in Weitkamp, C. (ed.), [Lidar: Range-Resolved Optical Remote Sensing of the Atmosphere], Springer, New York (2005). doi:10.1007/b106786

[8] Guan, Z. G., Lundin, P., Mei, L., Somesfalean, G. and Svanberg, S., "Vertical lidar sounding of atomic mercury and nitric oxide in a major Chinese city," Applied Physics B: Lasers and Optics 101(1–2), 465–470 (2010). doi:10.1007/s00340-010-4166-8

[9] Calpini, B. and Simeonov, V., "Trace Gas Species Detection in the Lower Atmosphere by Lidar: From Remote Sensing of Atmospheric Pollutants to Possible Air Pollution Abatement Strategies," in Fujii, T. and Fukuchi, T. (eds.), [Laser Remote Sensing], CRC Press, Boca Raton (2005).

[10] Robinson, R., Gardiner, T. D., Innocenti, F., Woods, P. T. and Coleman, M, "Infrared differential absorption lidar (DIAL) measurements of hydrocarbon emissions," Journal of Environmental Monitoring 13(8), 2213–2220 (2011). doi:10.1039/c0em00312c

[11] Johnson, W., Repasky, K. S. and Carlsten, J. L., "Micropulse differential absorption lidar for identification of carbon sequestration site leakage," Applied Optics 52(13), 2994–3003 (2013). doi:10.1364/AO.52.002994

[12] Ikuta, K., Yoshikane, N., Vasa, N., Oki, Y., Maeda, M., Uchiumi, M., Tsumura, Y., Nakagawa, J. and Kawada, N., "Differential absorption lidar at 1.67 μm for remote sensing of methane leakage," Japanese Journal of Applied Physics Part 1 38, 110–114 (1999). doi:10.1143/JJAP.38.110

[13] Rothman, L. S. et al., "The HITRAN 2008 molecular spectroscopic database," Journal of Quantitative Spectroscopy & Radiative Transfer 110(9–10), 533–572 (2009). doi:10.1016/j.jqsrt.2009.02.013

[14] [Safety of Laser Products], British Standards Institute, BS EN 60825-1:2007 (2007).

[15] Gibert, F., Flamant, P., Bruneau, D. and Loth, C., "Two-micrometer heterodyne differential absorption lidar measurements of the atmospheric CO_2 mixing ratio in the boundary layer," Applied Optics 45(18), 4448–4458 (2006). doi:10.1364/AO.45.004448

[16] Refaat, T. F., Ismail, S., Koch, G. J., Rubio, M., Mack, T. L., Notari, A., Collins, J. E., Lewis, J., De Young, R., Choi, Y., Abedin, M. N. and Singh, U. N., "Backscatter 2-μm lidar validation for atmospheric CO_2 differential absorption lidar applications," IEEE Transactions on Geoscience and Remote Sensing 49(1), 572–580 (2010). doi:10.1109/TGRS.2010.2055874

[17] Sakaizawa, D., Nagasawa, C., Nagai, T., Abo, M., Shibata, Y., Nakazato, M. and Sakai, T., "Development of a 1.6 μm differential absorption lidar with a quasi-phase-matching optical parametric oscillator and photon-counting detector for the vertical CO_2 profile," Applied Optics 48(4), 748–757 (2009). doi:10.1364/AO.48.000748

[18] Amediek, A., Fix, A., Wirth, M. and Ehret, G., "Development of an OPO system at 1.57 μm for integrated path DIAL measurement of atmospheric carbon dioxide," Applied Physics B 92(2), 295–302 (2008). doi:10.1007/s00340-008-3075-6
[19] Abshire, J. B., Riris, H., Allan, G. R., Weaver, C. J., Mao, J., Sun, X., Hasselbrack, W. E., Kawa, R. S. and Biraud, S., "Pulsed airborne lidar measurements of atmospheric CO_2 column absorption," Tellus Series B 62(5), 770–783 (2010). doi:10.1111/j.1600-0889.2010.00502.x
[20] Harvard–Smithsonian Centre for Astrophysics and V. E. Zuev Institute of Atmospheric Optics, "HITRAN on the Web," (23 April 2013). http://hitran.iao.ru/
[21] Kovalev, V. A., and Eichinger, W. E., "Elastic Lidar: Theory, Practice, and Analysis Methods," John Wiley & Sons, Hoboken (2004). doi:10.1002/0471643173
[22] Lavrov, A., Utkin, A. B., and Vilar, R., "Simple eye-safe lidar for cloud height measurement and small forest fire detection," Optics and Spectroscopy 109(1), 144–150 (2010). doi:10.1134/S0030400X10070246
[23] Oke, T. R., [Boundary Layer Climates], second edition, Routledge, London (1999).
[24] Numata, K., Chen, J. R., Wu, S. T., Abshire, J. B., and Krainak, M. A. "Frequency stabilization of distributed-feedback laser diodes at 1572 nm for lidar measurements of atmospheric carbon dioxide," Applied Optics 50(7), 1047–1056 (2011). doi:10.1364/AO.50.001047